An investigation of nanostructured thin film α-MoO_3 based supercapacitor electrodes in an aqueous electrolyte

Beatriz Mendoza-Sánchez [a,*], Thierry Brousse [b], Claudia Ramirez-Castro [b], Valeria Nicolosi [a,1], Patrick S. Grant [a]

[a] Department of Materials, University of Oxford, Parks Road, Oxford OX1 3PH, United Kingdom
[b] Institut des Matériaux Jean Rouxel (IMN), Université de Nantes, CNRS, 2 rue de la Houssinière, BP 32229, 44322 Nantes Cedex 3, France

Abstract

The potential for MoO_3 use as a supercapacitor electrode in aqueous electrolytes was investigated. α-MoO_3 nanobelts were synthesized using a hydrothermal method and then thin-film electrodes were manufactured by spray deposition. Electrochemical testing in several aqueous electrolytes showed significant charge storage in 1 M H_2SO_4 with a complex electrochemical activity that was further investigated by X-ray photoelectron spectroscopy and various electrochemical characterization methods. In a 0–1 V (vs Ag/AgCl) electrochemical window, MoO_3 was reduced to a mixture of lower valence oxides with concentrations varying as Mo (5+) > Mo (4+) > Mo (6+), with MoO_2 as the main component at potentials below 0.185 V (vs Ag/AgCl). The degree of redox reversibility was evaluated in order to optimize the electrochemical window for enhanced cyclability. A moderate capacitance of 8.8 F g^{-1} (64 μF cm^{-2}) was fully retained for 720 cycles in an optimized electrochemical window of 0.26–0.43 V (vs Ag/AgCl).

Keywords

- α-MoO_3 nanobelts;
- Supercapacitors;
- Redox activity;
- Capacitance;
- Cyclability

1. Introduction

Supercapacitors can store energy by two mechanisms: a charge separation at an electrode–electrolyte interface known as double layer capacitance and by Faradaic charge transfer at the surface of the electroactive material known as pseudocapacitance. Transition metal oxides can be induced to exhibit pseudocapacitive behaviour and ruthenium oxide is the most widely explored due to its high theoretical and practically achievable pseduocapacitance [1–4]. However, its high cost and toxicity has prevented its widespread use and many alternative transition metal oxides have also been studied [5,6] including manganese oxide [7–19], vanadium oxide [20–22], iron oxides [23–28], and molybdenum oxides [29–34]. Of these, manganese oxide is the most studied and promising, although its performance is inferior to that of ruthenium oxide. Molybdenum is a metal with a wide range of oxidation states from +2 to +7 existing in a variety of oxides and other compounds [35,36], of which MoO_3 and MoO_2 have been of interest for supercapacitor applications due to a rich electrochemical activity, low cost, and environmentally friendly nature [29–34]. α-MoO_3 possess a layered orthorhombic crystal structure where each layer is linked to an adjacent layer by van der Waals forces along the [0 1 0] direction. Each layer is composed of two MoO_6 octahedron nets where octahedrons share O—O edges along the [0 0 1] direction and corners along the [1 0 0] direction [37,38]. α-MoO_3 thus has the attraction not only of multiple oxidation states but also its potential for ion intercalation in between the crystal layers. However, α-MoO_3 is a semiconductor, the kinetics of Faradaic charge transfer is slow and it has generally shown poor cycling behaviour in Li-ion battery applications [39–41]. Careful selection of suitable nanostructure, dimensions, and crystal orientation, especially if intercalation (and associated strains) is present, can be used to improve the overall energy density and the cyclability of transition metal oxides supercapacitor electrodes [27,42]. Nanostructuring of α-MoO_3 increases its electroactive surface area and shortens diffusion lengths to promote faster ion transport.

Nanostructured α-MoO_3 and MoO_2 have been investigated for their application as supercapacitor electrodes in half cell arrangements in neutral (Na_2SO_4), basic (NaOH), and acidic electrolytes (H_2SO_4) [29–34]. Reports to date have described a variety of cyclic voltammetry (CV) responses in different electrochemical windows where attention has been paid mainly to the total capacitance achieved with less emphasis on extended cycling performance and elucidation of the underpinning reaction mechanisms. Reports of MoO_3 and MoO_2 tested in Na_2SO_4 suggested both a double layer capacitive and a Na^+ intercalation pseudocapacitive contribution to overall capacitance but no attention was paid to the cause of the observed irreversibility [30,31]. Shakir et al. [33] proposed several charge storage mechanisms for α-MoO_3 tested in

* Corresponding author. Current address: Trinity College Dublin, Schools of Chemistry and Physics and CRANN, Dublin 2, Ireland.
E-mail address: mendozab@tcd.ie (B. Mendoza-Sánchez).
[1] Current address: Trinity College Dublin, Schools of Chemistry and Physics and CRANN, Dublin 2, Ireland.

1 M H_2SO_4: (1) Faradaic-like processes involving proton (H^+) and coupled electron insertion in a similar fashion to that found in RuO_2 [43,44]; (2) proton adsorption/desorption; and (3) intercalation of ions into the layered structure of MoO_3. However, there was no compelling experimental evidence providing an insight into one or more of the proposed mechanisms. Similarly, Farsi et al. [29] proposed a combination of a double layer capacitance combined with electron/proton insertion (mechanism 1) for electrodeposited molybdenum oxides tested in a mix of Na_2SO_4 and H_2SO_4 but in a different electrochemical window than suggested by Shakir et al. [33] and with no justification of their choice of electrolyte and electrochemical window. The multiple oxidation states of Mo provide MoO_3 with a rich redox activity in acidic electrolytes [36,45]. At the electrode surface, Mo (6+) is reduced to Mo (5+) in 1 M H_2SO_4. Pentavalent molybdenum oxide is a unstable compound with a characteristic blue colouration [46]. Stabilization of its crystal structure has been found to occur through the creation of oxygen vacancies followed by crystal relaxation [47,48] rather than the formation of molybdenum bronzes [49–52]. The reduction of Mo (5+) to Mo (4+) has been described as occurring through an intermediate unknown species by a combination of chemical and electrochemical reactions [47]. Overall the attractive richness of Mo oxidation states creates difficulties in elucidating the underlying mechanisms of Mo based oxide electrochemical activity in supercapacitor applications, and significant uncertainties remain. In this work α-MoO_3 nanobelts with a crystalline nanostructure were synthesized using a hydrothermal method, and binder-free, nanometer-thick electrodes with enhanced mechanical stability were fabricated using a spray deposition technique. The α-MoO_3 nanobelts electrodes were tested in several electrolytes finding an enhanced charge storage in 1 M H_2SO_4 where a series of cathodic and anodic peaks underscored the complex redox activity described above. Insights into the redox activity were gained by using X-ray photoelectron spectroscopy (XPS) combined with electrochemical characterization methods, and led to an improvement of the performance of α-MoO_3 as a supercapacitor electrode.

2. Experimental

2.1. Materials

Elicarb single walled carbon nanotubes (SWNTs) were supplied by *Thomas Swan and Co. Ltd (UK)*; Mo powder (99.9 %), and hydrogen peroxide (30 %) by *Sigma Aldrich (UK)*; poly(ethyleneimine) (PEI, Mw = 70,000) by *Alfa-Aesar (UK)*. Deionized water (10 MΩ cm) was used for all processing.

2.2. α-MoO_3 nanobelt synthesis

α-MoO_3 nanobelts were synthesized by a hydrothermal method previously described by Hu et al. [53]. A colloidal suspension of peroxomolybdic acid was obtained by gradually adding Mo powder (4 g, 41.7 mmol) to H_2O_2 (30%, 40 ml) under gentle agitation and ice cooling. The colloidal suspension was then transferred to a teflon lined autoclave and maintained at 180 °C for 48 h. Subsequently the autoclave was cooled down to room temperature and the solid product was extensively rinsed with deionized water while vacuum filtrating. The solid was then collected and dried at 60 °C in vacuum oven.

2.3. α-MoO_3 nanobelt aqueous suspensions

An aqueous suspension of α-MoO_3 (0.1–0.5 mg ml^{-1}) nanobelts was produced by ultrasonication (100 W, 30 kHz, small tip) for 5 min.

2.4. Electrode manufacture

Electrodes of 1 cm^2 area were spray-deposited onto indium tin oxide (ITO) coated glass substrates (7 Ω/sq sheet resistance) by a method described elsewhere [54,55]. Briefly, suspensions of electrochemically active material were fed into a industrial spray head where an atomizing air flow produced a suspension mist that was deposited onto a substrate maintained at a temperature suitable for the immediate volatilization of the fugitive carrier liquid (water). The spray head was moved at a constant spray height and speed in a single direction above the target substrates to produce films of uniform thickness over the entire substrate area. Prior to the spray deposition of electroactive material, substrates were precoated with a 5 nm layer of 0.1 %, w/w PEI solution to improve adhesion of the electroactive material to the substrate. Films of α-MoO_3 nanobelts were manufactured by spray deposition of 150 ml of a 0.13 mg ml^{-1} aqueous supension. The average mass and thickness of α-MoO_3 nanobelts electrodes were 0.08–0.15 mg, and 500 nm respectively.

2.5. Equipment and characterization techniques

Transmission electron microscopy (TEM) images were obtained with a *JEOL 2010* operated at 200 kV; scanning electron microscopy (SEM) images were obtained in a field emission *FESEM JEOL 840 F* operated at 5 kV and a 15 mm working distance; X-ray diffraction (XRD) was performed in a Siemens D5000 powder diffractometer equipped with a monochromatic Cu Kα radiation source (λ = 0.15406 nm) and a secondary monochromator. XRD patterns were collected between $5° < 2\theta < 75°$, with a step size of $2\theta = 0.05°$ and a count time of 12 s/step. X-ray photoelectron spectroscopy (XPS) was performed in a *Kratos Axis Ultra* spectrometer equipped with a monochromatic Al Kα (1486.6 eV) as the source and with a spot size 0.7 × 0.3 mm^2. The C_{1s} (sp^2) binding energy (284.9 eV) was used as reference for XPS spectra calibration. The XPS spectra were analyzed and fitted using CasaXPS software. A mixture of Gaussian and Lorentzian functions was used for the least-squares curve fitting procedure. Ultrasonication was performed in a ultrasonicator *UP100H, Hielscher* (100 W, 30 kHz), and a *Sonics Vibra cell VC-600-2* probe (600 W, 20 kHz). Electrode thickness was determined by step height measurements in a Dektak 6M profilometer (*Veeco Instruments, Inc.*) and the weight of deposited films was measured using a *Sartorius* microbalance with 0.01 mg readability.

2.6. Electrochemical characterization

α-MoO_3 based thin film electrodes were tested in a three-electrode electrochemical cell configuration using a *Reference 600/EIS300 Gamry* potentiostat/galvanostat, Ag/AgCl electrode as reference – all potentials are reported vs Ag/AgCl, although in some cases and for the sake of comparison with the literature, potentials are reported both vs Ag/AgCl (0.197 V vs NHE) and another reference electrode such as Hg/Hg_2SO_4 (0.68 V vs NHE) or NHE –, a platinum sheet as counter electrode, and 1 M H_2SO_4 as the electrolyte (initial tests were also performed in 1 M Na_2SO_4, K_2SO_4, and Li_2SO_4 aqueous solutions). Most of the cyclic voltammetry experiments were performed in a potential range from 0 to 1 V vs Ag/AgCl where oxido-reduction process of interest take place.

3. Results and discussion

3.1. Material characterization

Fig. 1a shows the X-ray diffraction pattern of the as prepared material. The indexing of the distinct and sharp peaks identified highly crystalline and pure α-MoO_3 phase with an orthorhombic

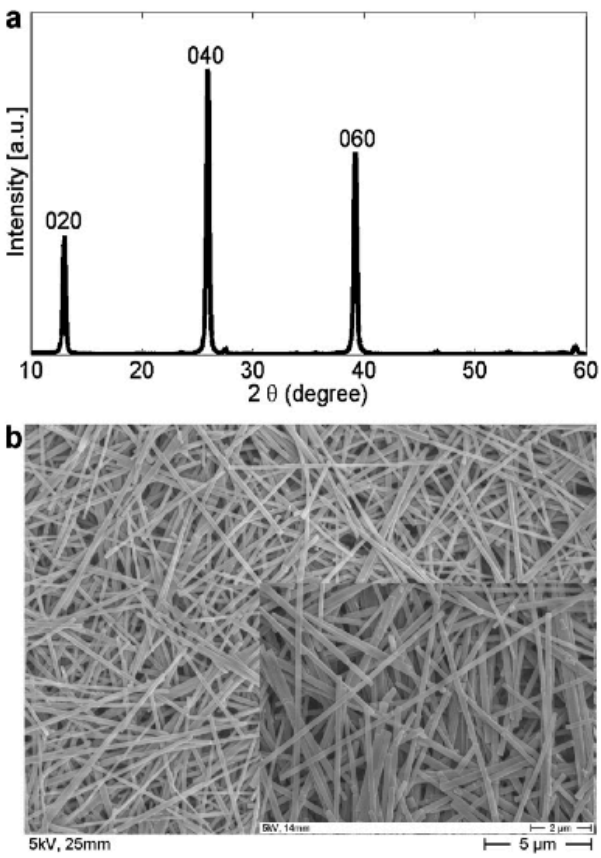

Fig. 1. (a) XRD pattern and (b) SEM image of as made α-MoO_3 nanobelts.

layered crystal structure (ICDD-JCPDS card No. 05-0508). The strong diffraction peaks from planes (0 k 0) showed a characteristic anisotropic growth of the α-MoO_3 phase [38,56]. Fig. 1b shows corresponding SEM images of the α-MoO_3 indicating largely a 1D elongated morphology with average dimensions of 300–400 nm width and 8–18 μm length. Because the width of the α-MoO_3 nanostructures was larger than the thickness, the nanocrystals were designated as nanobelts rather than nanorods. A TEM image and corresponding selected area electron diffraction (SAED) pattern of an individual α-MoO_3 nanobelt are shown in Fig. 2a and b. The SAED pattern, recorded perpendicular to the growth axis, was identified as the [0 1 0] zone axis indicating that growth of the nanobelts was primarily along the [0 0 1] direction. The HRTEM image in 2c indicated interplanar distances of 0.4 and 0.36 nm for the (1 0 0) and (0 0 1) lattice planes respectively. As shown in Fig. 1b, the combination of sonication followed by spray deposition allowed for the manufacture of electrodes consisting of a highly interconnected open network of α-MoO_3 nanobelts. The surface area of the α-MoO_3 was determined as 13.7 $m^2\ g^{-1}$ by nitrogen adsorption isotherms using the Brunauer–Emmett–Teller (BET) method.

3.2. Cyclic voltammetry

Fig. 3 shows a typical cyclic voltammogram (CV) of a spray-deposited α-MoO_3 electrode in 1 M H_2SO_4 at 10 mV s^{-1}, where a capacitance of 12.7 F g^{-1} was obtained. There was a complex electrochemical activity with several anodic (a) and cathodic (c) peaks: a_1 (487.3 mV), a_2 (391.2 mV), a_3 (242 mV); and c_1 (454.1 mV), c_2 (354.7 mV), c_3 (195.2 mV). Sulphuric acid was selected here as the electrolyte that provided the larger charge storage after electrodes were tested in other electrolytes including Na_2SO_4, K_2SO_4, and

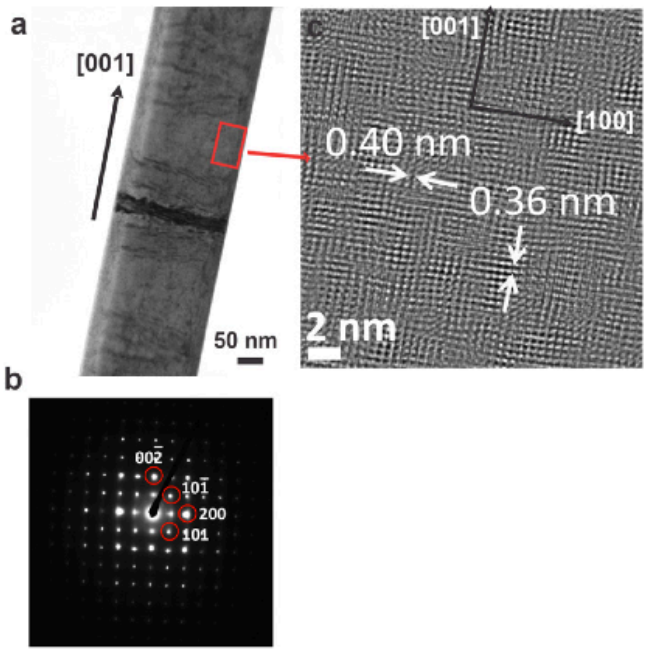

Fig. 2. (a) TEM image of a single α-MoO_3 nanobelt and (b) corresponding SAED pattern. (c) HRTEM image of enclosed nanobelt area showing interplanar distances along the [0 0 1] and [1 0 0] directions.

Li_2SO_4 and in which cases, there was only double layer capacitance (< 5 F g^{-1}) in the same electrochemical window of 0–1 V. A negative electrochemical window rendered either a lower charge storage and/or increased irreversibility (see Section 3.4).

3.3. XPS surface characterization of the electrodes

In order to investigate further the electrochemical activity of α-MoO_3 electrodes in 1 M H_2SO_4 in the 0–1 V electrochemical window (vs Ag/AgCl), XPS studies were performed in conjunction with cyclic voltammetry and chronoamperometry. This method was used successfully to elucidate the charge storage mechanisms in MnO_2 thin film electrodes for electrochemical capacitors [16]. Prior to XPS measurements, electrodes were subjected to polarization: cyclic voltammetry was performed at 20 mV s^{-1} from open circuit potential (OCP ≈ 0.34 V) up to the polarization potential $0 \leq E \leq 1$ V (either in reduction or oxidation) at which point the electrode was held at constant potential via chronoamperometry until the

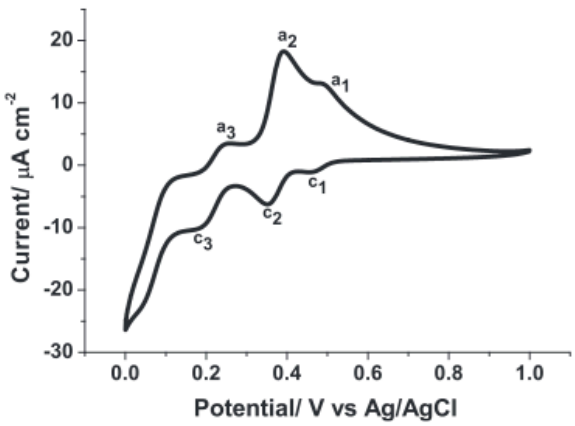

Fig. 3. Representative cyclic voltammogram of an α-MoO_3 electrode in 1 M H_2SO_4 at a scan rate of 10 mV s^{-1}. Labels identify anodic (a) and cathodic (c) redox peaks.

Table 1
Percentage concentration (± 3.0 %) of the spin–orbit components in the Mo 3d XPS binding energy region for electrodes polarized at various potentials *E*. *R* and *O* indicate polarization in reduction and oxidation respectively.

E (V vs Ag/AgCl)	0^R	0.13^R	0.185^R	0.26^R	0.415^R	0.3^O	0.46^O	1^O
Mo 3d 5/2 (4+)	22.7	23.3	19.0	8.7	5.3	6.8	4.8	6.8
Mo 3d 5/2 (5+)	29.3	28.3	37.8	45.7	50.9	43.1	48.7	47.5
Mo 3d 5/2 (6+)	2.9	3.9	2.5	7.5	4.1	11.5	6.8	7.2
Mo 3d 3/2 (4+)	21.2	19.7	16.3	4.5	4.0	4.1	3.6	3.5
Mo 3d 3/2 (5+)	19.5	22.2	21.7	28.05	29.3	25.1	31.7	32.6
Mo 3d 3/2 (6+)	4.6	2.6	2.8	5.7	6.2	9.3	4.4	2.4

current (I)–time (t) response reached a nearly steady state with $I \approx 0$. The chosen polarization potentials E (vs Ag/AgCl) are indicated in Fig. 6b and summarized in the headings of Table 1. A different sample was used for each polarization potential.

The polarization procedure of the electrodes can be understood by following Fig. 6b where anodic/cathodic peaks and polarization potentials are shown. For the case of polarization in reduction (red dots in Fig. 6b), and considering for instance the polarization at $E = 0.415$ V, a CV was run from OCP up to 1 V in oxidation, then down to the polarization potential $E = 0.415$ V in reduction (clockwise direction from OCP) at which point the chronoamperogram was run, hence the overall test involved a_2, a_1, and c_1 peaks in that sequence. In the case of the polarization in oxidation (blue dots in Fig. 6b), for polarization at $E = 0.3$ V for instance, the CV was run from OCP to $E = 1$ V in oxidation, then down to $E = 0$ V in reduction, and then up to $E = 0.3$ V in oxidation overall involving a_2, a_1, c_1, c_2, c_3, and a_3 peaks in that sequence. Summarizing, each polarization experiment describes: (1) the electrochemical activity occurring during the CV scan from OCP up to the particular polarization potential in question and (2) the particular event of reduction or oxidation at the specific polarization potential.

Fig. 4 shows the XPS spectrum in the Mo 3d binding energy region for an as prepared sample of α-MoO_3 nanobelts with two well resolved spectral lines which after curve fitting were identified as the characteristic Mo 3d spin–orbit doublet peaks of MoO_3: Mo $3d_{5/2}$ 6+at 232.6 eV and Mo $3d_{3/2}$ 6+at 235.7 eV [57,58]. This spectrum confirmed the purity of the α-MoO_3 phase of as-manufactured electrodes and provided a useful baseline against which the effect of various polarizations could be assessed.

For the α-MoO_3 electrodes then polarized at the different potentials E given in the headings of Table 1, curve fitting of XPS spectrum in the Mo 3d binding energy region suggested the presence of three spin–orbit doublets corresponding to three species. Fig. 5 shows the Mo 3d XPS spectra for α-MoO_3 electrodes polarized at $E = 1$ V and $E = 0$ V. For the α-MoO_3 electrode polarized at $E = 1$ V, spin–orbit components were assigned as: 230.0 eV (Mo $3d_{5/2}$ 4+), 231.2 eV (Mo $3d_{5/2}$ 5+), 231.8 eV (Mo $3d_{5/2}$ 6+), 233.0 eV Mo $3d_{3/2}$ 4+), 234.3 eV (Mo $3d_{3/2}$ 5+) and 235.1 eV (Mo $3d_{3/2}$ 6+). For the α-MoO_3 electrode polarized at $E = 0$ V, spin–orbit components were assigned as: 229.7 eV (Mo $3d_{5/2}$ 4+), 231.1 eV (Mo $3d_{5/2}$ 5+), 231.5 eV (Mo $3d_{5/2}$ 6+), 232.8 eV (Mo $3d_{3/2}$ 4+), 234.3 eV (Mo $3d_{3/2}$ 5+) and 235.6 eV (Mo $3d_{3/2}$ 6+). A spin–orbit component corresponding to S 2s at 231.1 eV was also identified, attributed to SO_4^{2-} ions (see below the analysis of the O 1s binding energy region) and with a percentage peak area < 5 % and therefore considered negligible for the following analysis. For α-MoO_3 electrodes polarized at each of the other potentials, the Mo 3d XPS spectrum showed spin–orbit components at similar

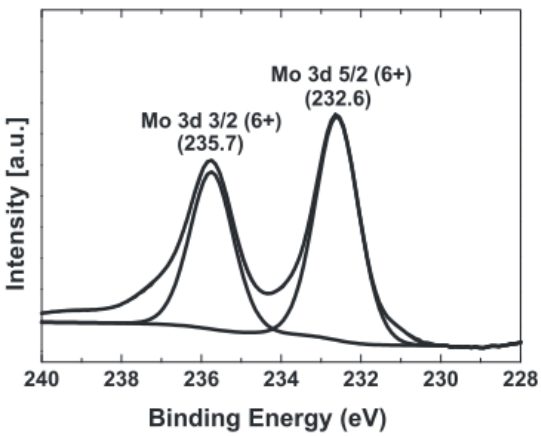

Fig. 4. XPS spectrum in the Mo 3d binding energy region of as made α-MoO_3 nanobelts.

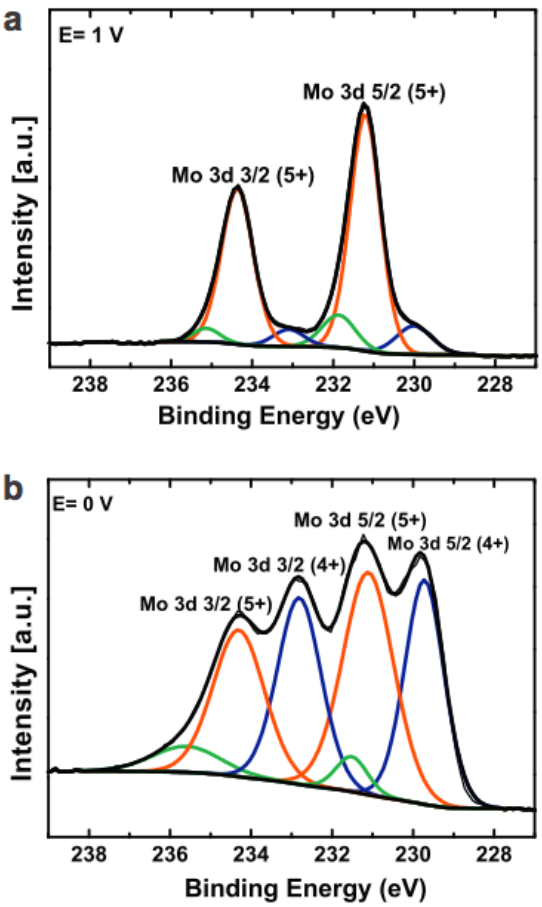

Fig. 5. XPS spectra in the Mo 3d binding energy region of α-MoO_3 electrodes polarized at (a) $E = 1$ V and (b) $E = 0$ V. Spin–orbit components are shown in green for Mo 3d (6+), red for Mo 3d (5+), and blue for Mo 3d (4+). (For interpretation of references to colour in this figure legend, the reader is referred to the web version of this article.)

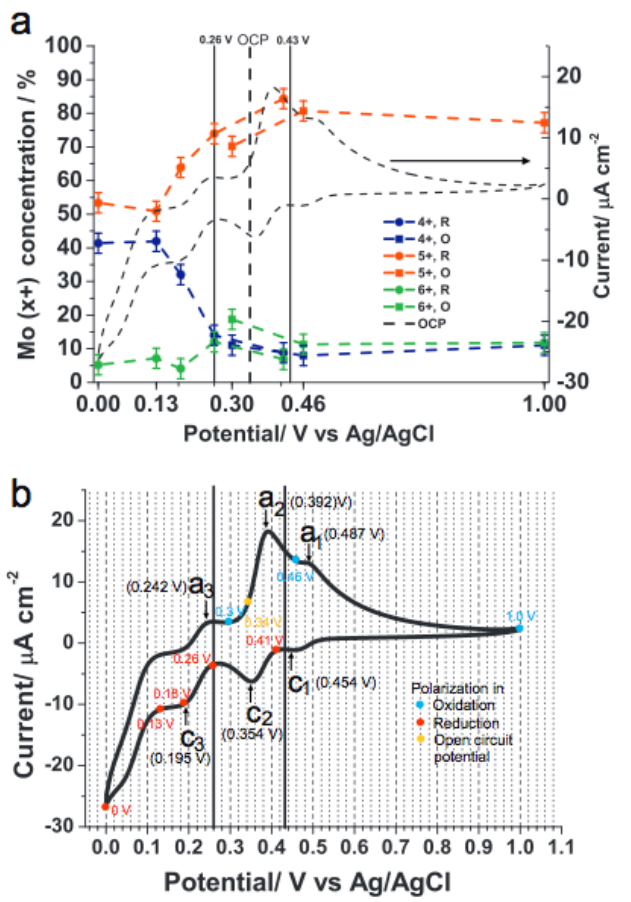

Fig. 6. (a) Plot showing the percentage concentration of Mo (x+) at the surface of polarized α-MoO_3 electrodes vs polarization potentials E. The percentage concentration of each Mo (x+) species has been calculated from the area integration of the corresponding Mo $3d_{5/2}$ (x+) XPS spin–orbit component. Dashed lines joining the data points are for visual guide. The electrodes have been scanned from open circuit potential OCP, shown for reference as a dashed black line, up to polarization potential E either in reduction (R, circles) or oxidation (O, squares). Error bars show a ± 3 % error, (b) cyclic voltammogram showing polarization potentials E in reduction (red) and oxidation (blue), also summarized in Table 1, and OCP (yellow). The limits of a selected electrochemical window (0.26–0.43 V) are indicated by black solid lines in (a) and (b). The cyclic voltammogram is also shown in (a) in dashed lines in order to correlate the changes in oxidation state with cathodic and anodic peaks. (For interpretation of references to colour in this figure legend, the reader is referred to the web version of this article.)

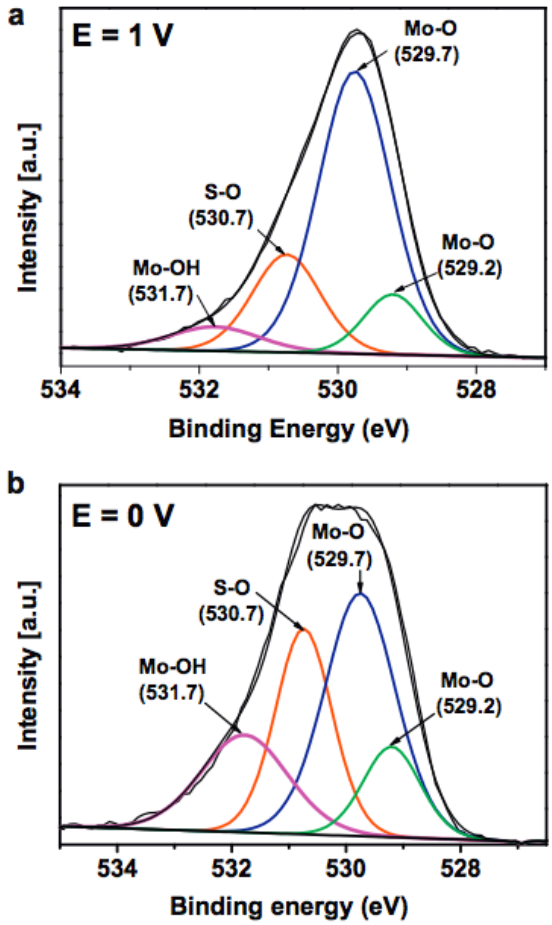

Fig. 7. XPS spectra in the O 1s binding energy region of α-MoO_3 electrodes polarized at (a) $E = 1$ V and (b) $E = 0$ V.

binding energies. Table 1 shows the percentage concentration of each spin–orbit component for all the polarized electrodes.

The percentage concentration of the different Mo oxidation states were estimated by integration of the area under the Mo $3d_{5/2}$ and Mo $3d_{3/2}$ peaks separately. There were similar trends for both Mo 3d spin–orbit components. Fig. 6a shows data for the Mo $3d_{5/2}$ spin–orbit component where Mo(4+)/Mo(5+)/Mo(6+) concentration percentages were 11.0 ± 3.0 %/77.2 ± 3.0 %/11.8 ± 3.0 %, and 41.3 ± 3.0 %/53.4 ± 3.0 %/5.2 ± 3.0 % for $E = 1$ V and $E = 0$ V, respectively. At $E = 1$ V, the major species was Mo (5+), whereas at $E = 0$ V a decrease of concentration of Mo (5+) was accompanied by an increase in the concentration of Mo (4+). As shown in Fig. 5, a shift by 0.3 V of the XPS Mo 3d spectra of the electrode held at $E = 0$ V provided further supporting evidence for the reduction to Mo (4+). The CV at 10 mV s^{-1} in Fig. 6a (dashed) and further detailed in Fig. 6b is shown to correlate the oxido-reduction events with anodic and cathodic peaks. The increase of concentration percentage of Mo (4+) coupled to a decrease in concentration percentage of Mo (5+) was a trend observed for polarization potentials in reduction < $E = 0.26$ V and was clearly enhanced for potentials $E = 0.185$ V, $E = 0.13$ V, and $E = 0.0$ V indicating that the cathodic peak c_3 was involved in such reduction process. Polarizations in oxidation at $E = 0.3$ V, $E = 0.46$ V, and $E = 1.0$ V all showed the same trend of concentration percentages of Mo oxidation states as Mo (5+) > Mo (6+) > Mo (4+) suggesting that the anodic peaks a_3, a_2, and a_1 were involved in the oxidation of Mo (4+) to Mo (5+).

Fig. 7 shows the O 1s XPS spectra for electrodes held at $E = 1$ V and $E = 0$ V. Curve fitting showed four species with binding energy peaks at 529.20 eV, 529.7 eV, 530.7 eV and 531.7 eV assigned to Mo—O, Mo—O, S—O, and Mo—OH bonds respectively. Molybdenum—oxygen bonds are known to appear at 529–530 eV [57,59] with similar binding energies for MoO_3 and MoO_2 respectively [57]. The presence of a metal—hydroxyl bond at ≈ 531 eV has been reported not only for molybdenum oxides (Mo—OH) [59] but also for iron oxides (Fe–OH) [60], and manganese oxides (Mn—OH) [16]. The presence of sulphur on the samples was detected on the survey spectrum as the S 2p orbital at 168.0 eV and was attributed to the presence of SO_4^{2-} ions coming from the electrolyte, hence the consideration of a S—O bond component in the O 1s spectrum.

In summary, spectro-electrochemical experiments showed that during cyclic voltammetry in 1 M H_2SO_4 from 0 to 1 V, MoO_3 was partially reduced to a mix of oxides of lower oxidation states with relative electrode surface concentrations: Mo (5+) > Mo (4+) > Mo (6+). There was a reduction to Mo (4+) at potentials $E = 0.185$ V and $E = 0$ V and this was in agreement with data provided by the

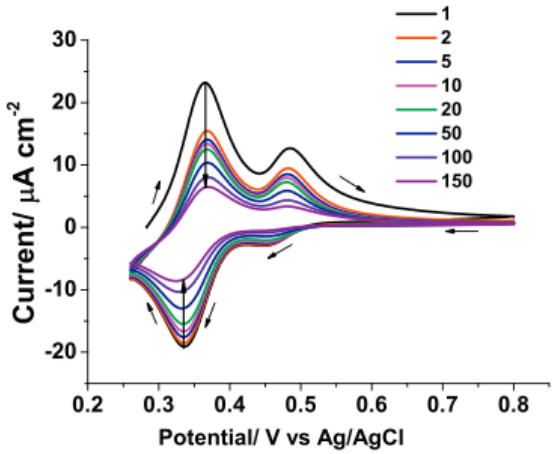

Fig. 8. Cyclic voltammogram of an α-MoO_3 electrode in 1 M H_2SO_4 at a scan rate of 20 mV s^{-1} in a 0.26–0.8 V electrochemical window showing cycles 1, 2, 5, 10, 20, 50, 100, and 150. The small arrows show the scanning direction and the large arrows show the peak current decrease upon cycling.

Pourbaix diagram [45] for the Mo–water system at pH = 0 where the prevalent Mo compound at 0.32 V (vs NHE)/0.12 V (vs Ag/AgCl) is MoO_2. Earlier investigations based on cyclic voltammetry at 5 mV s^{-1} determined an electrochemical reduction of Mo (6+) to Mo (5+) at −240 mV vs Hg/Hg_2SO_4 (237 mV vs Ag/AgCl) with the appearance of a dark blue colouration attributed to an oxygen-deficient oxide rather than the formation of hydrogen molybdenum bronzes (H_xMoO_3) [47,48]:

$$2MoO_3 + 2H^+ + 2e^- \rightarrow Mo_2O_5 + H_20 \quad (1)$$

The formation of hydrogen molybdenum bronzes H_xMoO_3 – leading to dissolution in 0.5 M H_2SO_4 – has been reported within a 80 mV to −555 mV (vs Ag/AgCl) electrochemical window with the appearance of four different phases at scan rates below 2 mV s^{-1}, above which the associated redox peaks disappeared [49–51,61]. Since the scan rate here used was 20 mV s^{-1} along with a 0–1 V (vs Ag/AgCl) electrochemical window, the formation of even phase II ($H_{1.04}MoO_3$) at 80 mV (vs Ag/AgCl) was unlikely.

It has been also reported that direct reduction of Mo (5+) to Mo (4+) (brown) was not possible and that the existence of an intermediate species, likely to be Mo (3+) (also dark blue), occurred at −400 mV vs Hg/Hg_2SO_4 (77 mV vs Ag/AgCl) with oxidation to MoO_2 at −475 mV vs Hg/Hg_2SO_4 (2 mV vs Ag/AgCl) [47,48]. The detection of MoO_2 by XPS along with the observation of a dark blue colouration in electrodes polarized at potentials $E = 0$ V, $E = 0.13$ V and $E = 0.185$ V in the present work, are supportive of the oxido-reduction processes described above [47,48]. In the case of Mo (6+), there was a low concentration that was approximately constant at all polarization potentials which may indicate a partial reoxidation in air to Mo (6+) or that there was an underlying layer of Mo (6+) in the electrode, still detectable by XPS, that remained

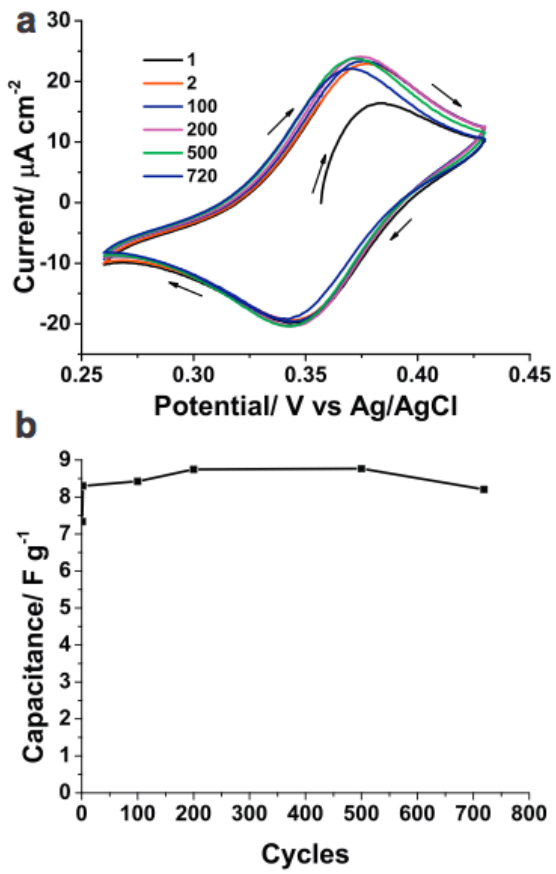

Fig. 9. (a) Cyclic voltammogram of an α-MoO_3 electrode in 1 M H_2SO_4 at a scan rate of 20 mV s^{-1} showing cycles 1, 2, 100, 200, 500 and 720 and (b) capacitance vs cycle number. The arrows indicate the scanning direction.

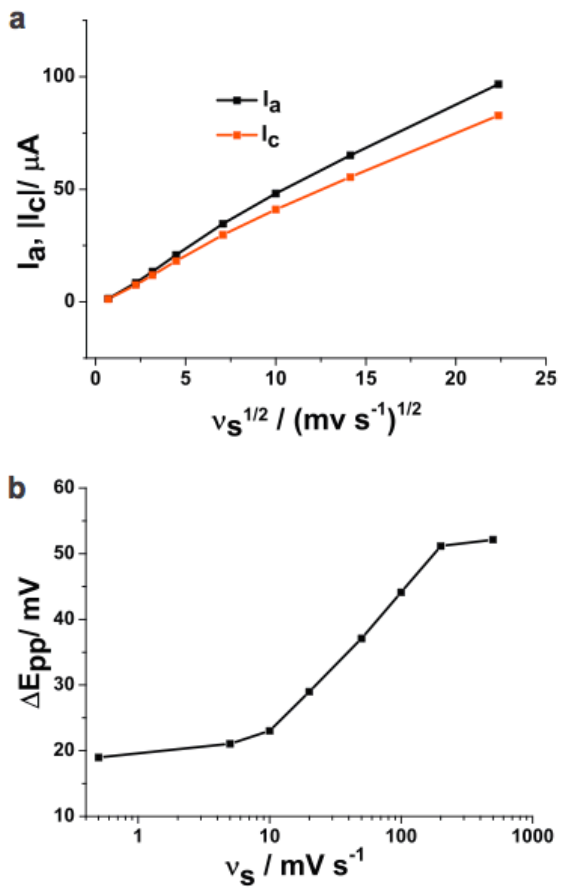

Fig. 10. Analysis of cyclic voltammograms in the optimized electrochemical window 0.26–0.43 V: (a) anodic (I_a) and cathodic (I_c) peak currents as function of the square root of scan rate ν and (b) peak-to-peak potential ΔE_{pp} as function of the logarithm of the scan rate.

electrochemically inactive. Further spectro-electrochemical studies will be needed to establish a complete reaction mechanism unambiguously, but the current work provides considerable support for the oxido-reduction processes previously reported [47,48].

3.4. Optimization of electrochemical window and cycling behaviour

On the basis of the XPS studies, optimization of the electrochemical window for improved reversibility was carried out. As shown in Fig. 6, potentials in the range 0 V < E < 0.26 V lead to irreversible reduction to MoO_2. An electrode tested by cyclic voltammetry in the potential range 0.26 V < E < 0.8 V showed a progressive decrease in charge storage capacity during 150 cycles, as shown in Fig. 8. The optimum reversibility – rather than absolute charge storage capacity on the first cycle – was achieved in the electrochemical window 0.26 V < E < 0.43 V involving redox peaks c_2 and a_2. Fig. 9 shows a cyclic voltammogram of an α-MoO_3 electrode swept within this electrochemical window with near constant capacitance and null charge storage capacity degradation after 720 cycles. A maximum capacitance of 8.8 F g^{-1} was obtained which is equivalent to 64 μF cm^{-2} when normalized per surface area (as measured by the BET method).

Cyclic voltammetry in the optimized electrochemical window at increasing scan rates allowed for further understanding of the electrochemical activity. Fig. 10a shows a linear dependence of the currents associated with anodic and cathodic peaks with the square root of the scan rate describing a process dominated by linear diffusion. If the electrochemical reactions were under diffusion control, it was likely that less accessible reaction sites in the interior of the electrode remained electrochemically inactive, and this may further support the earlier XPS findings of persistent non-reduced MoO_3.

The reversibility of the system was evaluated further considering the peak-to-peak potential difference of anodic and cathodic current peaks, ΔE_{pp}, as function of the logarithm of scan rate. In an ideally reversible system $\Delta E_{pp} \approx 57$ mV and is independent of scan rate [62]. As shown in Fig. 10b ΔE_{pp} < 57 mV for all scan rates and was approximately constant (≈ 20 mV) for scan rates ≤ 10 mV s^{-1}. Since MoO_3 is a n-type semiconductor, the rate of electron transport kinetics (measured by the standard electrochemical rate constant k°) is limited and thus the rate of mass transport $m_T \propto \nu^{1/2}$, where ν is the scan rate, becomes dominant at low scan rates leading to irreversibilities – in a reversible process $k^{\circ}/m_T \geq 15$ [62]. However, a stable charge storage capacity at 20 mV s^{-1} for 720 cycles, as demonstrated above, was indicative of a quasi-reversible behaviour at this scan rate.

Previous work reported electrodeposited molybdenum oxide tested by cyclic voltammetry in a 0.005 M H_2SO_4 + 0.095 M Na_2SO_4 electrolyte in a −0.55 to 0.0 V vs Ag/AgCl electrochemical window where the charge storage mechanism suggested was a combination of redox pseudocapacitance and double layer capacitance [29]. As shown in Fig. 11, testing of an α-MoO_3 electrode in the same electrochemical window and the same electrolyte showed a comparatively high capacitance obtained nevertheless at the expense of an obvious irreversible behaviour and consequently there was a marked capacitance degradation after only 60 cycles.

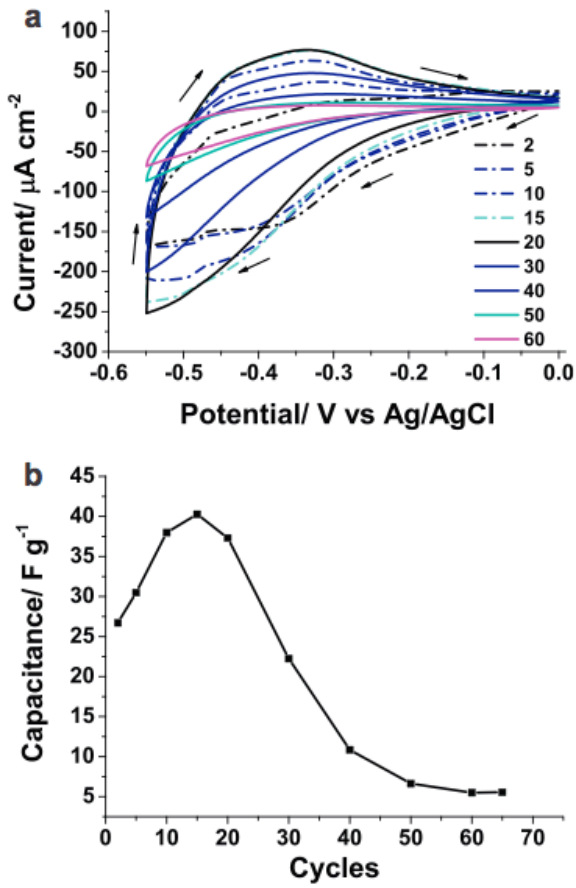

Fig. 11. (a) Cyclic voltammogram of an α-MoO_3 electrode in 0.005 M H_2SO_4 +0.095 M Na_2SO_4 at a scan rate of 5 mV s^{-1} showing cycles 2, 5, 10, 15, 20, 30, 40, 50 and 60. The current increases from cycles 2 to 20 (dashed lines), and decreases from cycles 20 to 60 (solid lines) and (b) capacitance vs cycle number. The arrows indicate the scanning direction.

4. Conclusions

The suitability of α-MoO_3 nanobelts for supercapacitor applications was examined in various aqueous electrolytes, finding the greatest charge storage and a rich redox activity in 1 M H_2SO_4. A combination of XPS with various electrochemical characterization methods revealed a partial reduction of MoO_3 to a mix of lower valence oxides with concentrations varying as Mo (5+) > Mo (4+) > Mo (6+) in a 0–1 V (vs Ag/AgCl) electrochemical window, and with MoO_2 as the species found at potentials below 0.185 V (vs Ag/AgCl). In the light of the redox changes occurring, the electrochemical window was optimized for enhanced reversibility obtaining a stable capacitance of 8.8 F g^{-1} (64 μF cm^{-2}) that was maintained up to 720 cycles. Thus for using α-MoO_3 as an electrochemical capacitor device, the potential window has to be drastically decreased at the expense of the absolute capacitance. Similarly, opening the potential window increased the capacitance but drastically lowered the cycling ability of the electrode.

Acknowledgements

The authors would like to thank financial support of the Mexican National Council of Science and Technology (CONACYT), UK Engineering and Physical Science Research Council (Supergen Energy Storage, EP/HO19596), and the Mathematics, Physical and Life Sciences division, Oxford University. Jonathan Hamon and Vincent Fernandez are acknowledged for their help with XPS measurements and analysis.

References

[1] H. Kim, B.N. Popov, Characterization of hydrous ruthenium oxide/carbon nanocomposite supercapacitors prepared by a colloidal method, Journal of Power Sources 104 (2002) 52.

[2] K.-H. Chang, C.-C. Hu, Oxidative synthesis of $RuO_2 \cdot nH_2O$ with ideal capacitive characteristics for supercapacitors, Journal of the Electrochemical Society 151 (2004) A958.
[3] P. Soudan, J. Gaudet, D. Guay, D. Bélanger, R. Schulz, Electrochemical properties of ruthenium-based nanocrystalline materials as electrodes for supercapacitors, Chemistry of Materials 14 (2002) 1210.
[4] K.M. Lin, K. Chang, C.C. Hu, Y.Y. Li, Mesoporous RuO_2 for the next generation supercapacitors with an ultrahigh power density, Electrochimica Acta 54 (2009) 4574.
[5] P. Simon, Y. Gogotsi, Materials for electrochemical capacitors, Nature Materials 7 (2008) 845.
[6] T. Cottineau, M. Toupin, T. Delahaye, T. Brousse, D. Bélanger, Nanostructured transition metal oxides for aqueous hybrid electrochemical supercapacitors, Applied Physics A: Materials Science and Processing 82 (2005) 599.
[7] H.Y. Lee, J.B. Goodenough, Supercapacitor behavior with KCl electrolyte, Journal of Solid State Chemistry 144 (1999) 220.
[8] S.-C. Pang, M.A. Anderson, T.W. Chapman, Novel electrode materials for thin-film ultracapacitors: Comparison of electrochemical properties of sol-gel-derived and electrodeposited manganese dioxide, Journal of the Electrochemical Society 147 (2000) 444.
[9] H.Y. Lee, S.W. Kim, H.Y. Lee, Expansion of active site area and improvement of kinetic reversibility in electrochemical pseudocapacitor electrode, Electrochemical and Solid-State Letters 4 (2001) A19.
[10] C.-C. Hu, T.-W. Tsou, Ideal capacitive behavior of hydrous manganese oxide prepared by anodic deposition, Electrochemistry Communications 4 (2002) 105.
[11] S.-F. Chin, S.-C. Pang, M.A. Anderson, Material and electrochemical characterization of tetrapropylammonium manganese oxide thin films as novel electrode materials for electrochemical capacitors, Journal of the Electrochemical Society 149 (2002) A379.
[12] J. Jiang, A. Kucernak, Electrochemical supercapacitor material based on manganese oxide: preparation and characterization, Electrochimica Acta 47 (2002) 2381.
[13] C.-C. Hu, T.-W. Tsou, Capacitive and textural characteristics of hydrous manganese oxide prepared by anodic deposition, Electrochimica Acta 47 (2002) 3523.
[14] J.-K. Chang, W.-T. Tsai, Material characterization and electrochemical performance of hydrous manganese oxide electrodes for use in electrochemical pseudocapacitors, Journal of the Electrochemical Society 150 (2003) A1333.
[15] R.N. Reddy, R.G. Reddy, Sol-gel MnO_2 as an electrode material for electrochemical capacitors, Journal of Power Sources 124 (2003) 330.
[16] M. Toupin, T. Brousse, D. Bélanger, Charge storage mechanism of MnO_2 electrode used in aqueous electrochemical capacitor, Chemistry of Materials 16 (2004) 3184.
[17] T. Brousse, M. Toupin, D. Bélanger, A hybrid activated carbon-manganese dioxide capacitor using a mild aqueous electrolyte, Journal of the Electrochemical Society 151 (2004) A614.
[18] J.-M. Luo, B. Gao, X.-G. Zhang, High capacitive performance of nanostructured Mn-Ni-Co oxide composites for supercapacitor, Materials Research Bulletin 43 (2008) 1119.
[19] L. Athouel, F. Moser, R. Dugas, O. Crosnier, D. Bélanger, T. Brousse, Variation of the MnO_2 birnessite structure upon charge/discharge in an electrochemical supercapacitor electrode in aqueous Na_2SO_4 electrolyte, Journal of Physical Chemistry C 112 (2008) 7270.
[20] H.Y. Lee, J.B. Goodenough, Ideal supercapacitor behavior of amorphous $V_2O_5 \cdot nH_2O$ in potassium chloride (KCl) aqueous solution, Journal of Solid State Chemistry 148 (1999) 81.
[21] T. Kudo, Y. Ikeda, T. Watanabe, M. Hibino, M. Miyayama, H. Abe, K. Kajita, Amorphous V_2O_5/carbon composites as electrochemical supercapacitor electrodes, Solid State Ionics 152–153 (2002) 833.
[22] C.M. Huang, C.C. Hu, K.H. Chang, J.M. Li, Y.F. Li, Pseudocapacitive characteristics of vanadium oxide deposits with a three-dimensional porous structure, Journal of the Electrochemical Society 156 (2009) A667.
[23] N.-L. Wu, S.-Y. Wang, C.-Y. Han, D.-S. Wu, L.-R. Shiue, Electrochemical capacitor of magnetite in aqueous electrolytes, Journal of Power Sources 113 (2003) 173.
[24] N.-L. Wu, Nanocrystalline oxide supercapacitors, Materials Chemistry and Physics 75 (2002) 6.
[25] S.Y. Wang, N.L. Wu, Operating characteristics of aqueous magnetite electrochemical capacitors, Journal of Applied Electrochemistry 33 (2003) 345.
[26] Z.H. Zhou, J. Wang, X. Liu, H.S.O. Chan, Synthesis of Fe_3O_4 nanoparticles from emulsions, Journal of Materials Chemistry 11 (2001) 1704.
[27] X. Zhao, B. Mendoza-Sánchez, P.J. Dobson, P.S. Grant, The role of nanomaterials in redox-based supercapacitors for next generation energy storage devices, Nanoscale 3 (2011) 839.
[28] X. Zhao, C. Johnston, P.S. Grant, A hybrid supercapacitor with carbon nanotube cathode and a hematite nanopowder/carbon naotube composite anode, Journal of Materials Chemistry 19 (2009) 8755.
[29] H. Farsi, F. Gobal, H. Raissi, S. Moghiminia, On the pseudocapacitive behavior of nanostructured molybdenum oxide, Journal of Solid State Electrochemistry 14 (2010) 643.
[30] L. Zheng, Y. Xu, D. Jin, Y. Xie, Well-aligned molybdenum oxide nanorods on metal substrates: solution-based synthesis and their electrochemical capacitor application, Journal of Materials Chemistry 20 (2010) 7135.
[31] F. Gao, L. Zhang, S. Huang, Fabrication horizontal aligned MoO_2/single-walled carbon nanotube nanowires for electrochemical supercapacitor, Materials Letters 64 (2010) 537.
[32] W. Sugimoto, T. Ohnuma, Y. Murakami, Y. Takasu, Molybdenum oxide/carbon composite electrodes as electrochemical supercapacitors, Electrochemical and Solid-State Letters 4 (2001) A145.
[33] I. Shakir, M. Shahid, H.W. Yang, D.J. Kang, Structural and electrochemical characterization of α-MoO_3 nanorod-based electrochemical energy storage devices, Electrochimica Acta 56 (2010) 376.
[34] R. Janarthanan, K. Pilli Satyananda, V. Balasubramanian, V. Thirukkallam Kanthadai, One-dimensional MoO_2 nanorods for supercapacitor applications, Electrochemistry Communications 11 (2009) 572.
[35] A.J. Bard, R.J.J. Parsons, Standard Potentials in Aqueous Solutions, Marcel Dekker, Inc., New York, USA, 1985.
[36] A.J. Bard, Encyclopedia of Electrochemistry of the Elements, Marcel Dekker, Inc., 1973, vol. 5, pp. 136–221.
[37] R.L. Smith, G.S. Rohrer, Scanning probe microscopy of cleaved molybdates: α-MoO_3(010), $Mo_{18}O_{52}$(100), Mo_8O_{23}(010), and η-Mo_4O_{11}(100), f Journal of Solid State Chemistry 124 (1996) 104.
[38] S.T. Wang, Y.G. Zhang, X.C. Ma, W.Z. Wang, X.B. Li, Z.D. Zhang, Y.T. Qian, Hydrothermal route to single crystalline α-MoO_3 nanobelts and hierarchical structures, Solid State Communications 136 (2005) 283.
[39] J.O.J. Heydecke, H.P. Fritz, Characteristics of molybdenum oxide and chromium oxide cathodes in primary and secondary organic electrolyte lithium batteries I. morphology, structure and their changes during discharge and cycling, Solid State Ionics 6 (1982) 215.
[40] J.O. Besenhard, J. Heydecke, E. Wudy, H.P. Fritz, W. Foag, Characteristics of molybdenum oxide and chromium oxide cathodes in primary and secondary organic electrolyte lithium batteries. Part II. transport properties, Solid State Ionics 8 (1983) 61.
[41] M.E. Spahr, P. Novak, O. Haas, R. Nesper, Electrochemical insertion of lithium, sodium, and magnesium in molybdenum(VI) oxide, Journal of Power Sources 54 (1995) 346.
[42] T. Brezesinski, J. Wang, S.H. Tolbert, B. Dunn, Ordered mesoporous α-MoO_3 with iso-oriented nanocrystalline walls, Nature Materials 9 (2010) 146.
[43] S. Hadzi-Jordanov, H. Angerstein-Kozlowska, M. Vukovic, B.E. Conway, Reversibility and growth behavior of surface oxide films at ruthenium electrodes, Journal of The Electrochemical Society 125 (1978) 1471.
[44] K.M. Lin, K. Chang, C.C. Hu, Y.Y. Li, Mesoporous RuO_2 for the next generation supercapacitors with an ultrahigh power density, Electrochimica Acta 54 (2009) 4574.
[45] M. Pourbaix, Atlas of Electrochemical Equilibria in Aqueous Solutions, Section 10, Pergamon Press, Oxford, New York, 1996.
[46] N.A. Dhas, A. Gedanken, Characterization of sonochemically prepared unsupported and silica-supported nanostructured pentavalent molybdenum oxide, Journal of Physical Chemistry B 101 (1997) 9495.
[47] N. Anbananthan, K. Nagaraja Rao, V.K. Venkatesan, Cyclic voltammetric investigations of the reduction of Mo(VI) to Mo(IV) in 1 M sulphuric acid, Journal of Electroanalytical Chemistry 374 (1994) 207.
[48] N. Anbananthan, K.N. Rao, V.K. Venkatesan, Electrochemical formation of oxygen-deficient molybdenum oxide, Applied Surface Science 72 (1993) 189.
[49] F. Endres, G. Schwitzgebel, Cyclic voltammetry of polyethylene stabilized hydrogen molybdenum bronzes, Journal of Electroanalytical Chemistry 415 (1996) 23.
[50] F. Endres, G. Schwitzgebel, Formation of secondary crystallites during electrochemical cycling of hydrogen molybdenum bronze, Materials Research Bulletin 31 (1996) 1537.
[51] F. Endres, G. Schwitzgebel, Impedance analysis of the phases I and III of hydrogen molybdenum bronze, Electrochimica Acta 43 (1998) 431.
[52] M. Greenblatt, Molybdenum oxide bronzes with quasi-low-dimensional properties, Chemical Reviews 88 (1988) 31.
[53] B. Hu, L. Mai, W. Chen, F. Yang, From MoO_3 nanobelts to MoO_2 nanorods: Structure transformation and electrical transport, ACS Nano 3 (2009) 478.
[54] B. Mendoza-Sánchez, L. Minati, P.S. Grant, Fourth European Symposium on Super Capacitors and Applications, Bordeaux, France, 2010.
[55] X. Zhao, B.T.T. Chu, B. Ballesteros, W.L. Wang, C. Johnston, J.M. Sykes, P. Grant, Spray deposition of steam treated and functionalized single-walled and multi-walled carbon nanotube films for super capacitors, Nanotechnology 20 (2009) 065605.
[56] G.S. Zakharova, C. Taschner, V.L. Volkov, I. Hellmann, R. Klingeler, A. Leonhardt, B. Buchner, $MoO_{3-\delta}$ nanorods: Synthesis, characterization and magnetic properties, Solid State Sciences 9 (2007) 1028.
[57] J.G. Choi, L.T. Thompson, XPS study of as-prepared and reduced molybdenum oxides, Applied Surface Science 93 (1996) 143.
[58] Z. Song, T. Cai, Z. Chang, G. Liu, J.A. Rodriguez, J. Hrbek, Molecular level study of the formation and the spread of MoO_3 on au (111) by scanning tunneling microscopy and x-ray photoelectron spectroscopy, Journal of the American Chemical Society 125 (2003) 8059.
[59] J. Torres, J.E. Alfonso, L.D. Lopez-Carreno, XPS and x-ray diffraction characterization of MoO_3 thin films prepared by laser evaporation, Physica Status Solidi C – Conference and Critical Reviews 2 (10) (2005) 3726.
[60] K. Asami, K. Hashimoto, S. Shimodaira, X-ray photoelectron spectrum of Fe^{2+} state in iron oxides, Corrosion Science 16 (1976) 35.
[61] D. Guay, G. Tourillon, G. Laperriere, D. Bélanger, Inuence of the electrolytic medium composition on the structural evolution of thin electrochromic molybdenum trioxide films probed by x-ray absorption spectroscopy, Journal of Physical Chemistry 96 (1992) 7718.
[62] R. Compton, C. Banks, Understanding Voltammetry, World Scientific Publishing Co., Pte. Ltd., Oxford, UK, 2007.